science.sciencemag.org/cgi/content/full/science.aax7526/DC1

Supplementary Materials for

Spatiotemporal expansion of primary progenitor zones in the developing human cerebellum

Parthiv Haldipur, Kimberly A. Aldinger, Silvia Bernardo, Mei Deng, Andrew E. Timms, Lynne M. Overman, Conrad Winter, Steven N. Lisgo, Ferechte Razavi, Evelina Silvestri, Lucia Manganaro, Homa Adle-Biasette, Fabien Guilmiot, Rosa Russo, Debora Kidron, Patrick R. Hof, Dianne Gerrelli, Susan J. Lindsay, William B. Dobyns, Ian A. Glass, Paula Alexandre, Kathleen J. Millen*

*Corresponding author. Email: kathleen.millen@seattlechildrens.org

Published 17 October 2019 on *Science* First Release
DOI: 10.1126/science.aax7526

This PDF file includes:

Materials and Methods
Figs. S1 to S7
Table S1
Captions for Data S1 to S4
References

Other Supplementary Material for this manuscript includes the following:
(available at science.sciencemag.org/cgi/content/full/science.aax7526/DC1)

Data S1 to S4 (.xlsx)

Materials and Methods

Human tissue collection: All human cerebellar samples (84 normal, 14 Dandy Walker Malformation and 2 Cerebellar vermis hypoplasia) were obtained in accordance with approved IRB protocols at Seattle Children's Research Institute. All 3-20 post-conception week (pcw) tissue samples were collected by the Human Developmental Biology Resource (HDBR) located at University College London, and Newcastle University, United Kingdom, and the Brain Defects Birth Laboratory (BDRL) at the University of Washington, Seattle, WA. Mid- and late-gestation samples were part of an archival collection at the Hôpital Necker-Enfants Malades in Paris, France. Samples were collected with previous patient consent and in strict accordance with institutional and legal ethical guidelines. Embryonic samples were staged using the Carnegie staging system, while older samples were staged using foot length. The age of the sample is listed as post-conception weeks (pcw), which starts from the point at which fertilization took place. There is an approximate 2-week difference between pcw and gestational weeks (gw). Only tissues with no detectable cerebellar pathology following histopathological analyses were included as controls. All Dandy-Walker malformation and cerebellar vermis hypoplasia samples used in the study were also part of archival collections obtained from pathologists from Italy, France and Israel, all of whom are authors on this study. Cerebella were fixed in formalin (pH 7.6) and embedded in paraffin. Sagittal sections of 4-5 μm thickness were cut using a microtome (Leica RM 2135) and placed on Superfrost Plus white slides (VWR international, USA). Slides were stored at room temperature until immunostaining was performed.

Animals: Animal experimentation was carried out in accordance with the guidelines laid down by the Institutional Animal Care and Use Committee (IACUC), of Seattle Children's Research Institute, Seattle, WA, USA. CD1 mice were crossed and the day of plug was taken as embryonic

day (E) 0.5. Embryos were dissected out between E12.5 and E16.5. Cerebella were dissected postnatally between P0 and P21. Samples were fixed in 4% paraformaldehyde (PFA) overnight, washed in PBS and sunk in 30% sucrose. Tissue was subsequently embedded in optimum cutting temperature (OCT) compound and midsagittal cryosections of 11 µm were collected. Images of the developing rhesus macaque cerebellum were obtained from the MacBrain resource (https://medicine.yale.edu/neuroscience/macbrain/), an extensive archival collection of macaque brain samples collected by Drs Rakic and Goldman-Rakic at the Department of Neuroscience at Yale University.

Histology: Human cerebellar tissue was fixed in 4% PFA and then processed through graded alcohols and changes of xylene and paraffin wax. Processed tissue was then embedded in paraffin wax prior to sectioning. Samples sectioned using the cryostat were treated with 30% sucrose following fixation. Paraffin sections were collected at 4 µm, while cryosections were collected at 12 µm. Cresyl violet, and Hematoxylin and Eosin (H&E) staining were carried out as previously described (*11*).

Immunohistochemistry: Immunohistochemistry was performed as previously described (*11*)**.** Briefly, sections were subjected to heat mediated antigen retrieval followed by blocking and permeabilization with 5% normal goat serum (Vector laboratories, S-1000) containing 0.35% triton X. Primary antibodies were incubated overnight at 4ºC. We used primary antibodies against KI67 (DAKO, M7240, mouse, 1:50), SOX2 (Thermofisher, PA1-094, Rabbit, 1:200), β-III Tubulin (Promega, G712A, Mouse, 1:1000), Calbindin (Swant, CD38, rabbit,1:3000), phospho-histone H3 (Cell signalling technologies, 9706S, rabbit, 1:100), CTIP1 (Abcam, ab19489, rabbit, 1:100), Wntless (Seven Hills Bioreagents, WLAB-177, rabbit, 1:100), PAX6

(Biolegend, 901301, rabbit, 1:300), TBR2 (Thermofisher, 14-4875-82, mouse,1:250), vimentin (Abcam, ab92547, rabbit, 1:200), GFAP (DAKO, Z0034, rabbit, 1:1000), CD34 (DAKO, M716501-2, Mouse, 1:100) and phospho-vimentin (MBL, D076-3, mouse, 1:200). Species and subtype-appropriate fluorescent dye-labelled secondary antibodies were used (Alexa Fluor 488 and 594, 1:1000, Molecular probes). Sections were counterstained with DAPI (4',6-diamidino-2-phenylindole) using Vectashield mounting medium with DAPI (Vector laboratories, H-1200).

***In situ* hybridization:** Assays were run using commercially available probes from Advanced Cell Diagnostics. Protocols recommended by the manufacturer were used without modification. The following probes were used in the study *LMX1A* (#540661), *MKI67* (#591771) and *ATOH1* (#417861). All sections were counterstained with fast green.

DiI/DiO and lentiviral labeling: DiI labeling was carried out as described in Saito et al. (*39*). Briefly, 500 µm- to 1 mm-thick sagittal slices of the cerebellum were collected from a 21 pcw cerebellum and incubated in DMEM medium containing fine crystals of DiI (D-282, Molecular Probes, USA) for 10-20 minutes on ice. Tissue was then washed in DMEM containing 10% fetal bovine serum and cultured overnight at 37^0C in 5% CO_2. Lentivirus expressing EGFP driven by spleen focus-forming virus (SFFV) promotor was also used for labeling human RL progenitors (*40*). This was provided by Dr Adrian Thrasher at University College London. Slices of 12 pcw cerebella were incubated with EGFP expressing lentivirus and cultured for 72 hours. Slices were then subsequently fixed in 4% PFA. Additionally, DiO crystals (D-275, Molecular Probes, USA) were placed in the VZ/SVZ region of fixed CS22 cerebellar slices. Slices were incubated were in 4% PFA for 4 weeks.

Microscopy: All slides from immunohistochemical assays were imaged using the Zeiss LSM-Meta confocal microscope and ZEN 2009 software (Zeiss). Brightfield microscopy was carried out at 20X magnification using a Nanozoomer Digital Pathology slide scanner (Hamamatsu; Bridgewater, New Jersey). Apart from minor adjustments of contrast and brightness to the entire image, there was no additional image alteration. All DiI and lentiviral treated slices were imaged using Zeiss LSM 880 confocal microscope fitted with a 20x water immersion objective with a numerical aperture (NA) of 0.95. All the images result from single z-plan or small projections of confocal Z-stacks created using ImageJ. To span the entire length of the neuroepithelia in Figure 2N we concatenated three images. Extra cells were occasionally removed from the field of view using Fiji to show examples of individual cells clearly and pseudo-coloring was used to highlight the cells of interest. Figures were prepared on Adobe Illustrator.

Laser-capture microdissection (LCM): The whole cerebellum was dissected from specimens that had intact calvaria to ensure correct orientation of the cerebellum **(Data S1)**. Intact cerebella were embedded in OCT, frozen at -80°C, and cryosectioned at 16-µm in the sagittal plane through the cerebellar vermis onto PEN Membrane Glass Slides (Applied Biosystems, USA). Total RNA was isolated from one whole section using the Qiagen RNeasy Micro Kit and RNA quality was assessed using the Agilent Bioanalyzer 6000 Pico Kit before proceeding with LCM. Mean RNA integrity number (RIN) was 7.63±0.79 (s.d.) among the 9 specimens. LCM was performed using the Leica DM LMD-6000 Laser Microdissection system to capture RL^{VZ} and RL^{SVZ} regions into separate collection tubes. Total RNA was then isolated from LCM-enriched samples pooled across each sample using the Qiagen RNeasy Micro Kit and RNA quality was assessed using the Agilent Bioanalyzer 6000 Pico Kit.

RNA sequencing: Sequencing libraries were prepared using the Illumina TruSeq RNA Access Prep Kit (Illumina, USA) and 25 ng of total RNA per sample (N=18), according to the manufacturer's protocol. RNA libraries were barcoded and sequenced including 6-8 samples per lane on an Illumina HiSeq 2000 by the Northwest Clinical Genomics Laboratory at the University of Washington. Paired-end reads (100 bp) were aligned to the *Human* reference genome (NCBI build 37/hg19) using STAR *(41)*. Genes counts were summarized using HTSeq *(42)*. Gene-level differential expression was analyzed using DESeq2 *(43)*. Genes with log2 fold change 1.5, *P* value < 0.05 and false discovery rate (FDR) < 0.05 were considered to be differentially expressed. Significant results are reported as Benjamini-Hochberg adjusted *P* values (FDR). Gene Ontology (GO) term and pathway enrichment analysis was performed using the STRING database of protein-protein interactions (https://string-db.org/) *(44)*. REVIGO (http://revigo.ibr.hr) was used to summarize GO results into non-redundant terms *(45)* **(Data S1-S4)**. Heatmaps were generated using the rlog normalized gene counts from DESeq2 and displayed using the R package pheatmap**.**

Cell counts: Cell counts were performed manually on Zen (PH3/pVIM) or Image J (KI67/SOX2). To study the proportion of mitotic ventricular to basal progenitors in the cerebellar VZ/SVZ the following number of cells were analyzed: Mouse = 154 (N=9, where N is the total number of biological replicates or samples analyzed), Human <CS18 = 239 (N=5), and Human > CS18 = 1560 (N=10). For the corresponding study in the mouse and human RL, the number of cells analyzed were as follows: Mouse = 23 (N=9), Human CS16-19 = 81 (N=7), and Human 10-18pcw = 291 (N=9). For KI67 and SOX2 counts, the total number of KI67 or SOX2+ cells relative to the total DAPI count in the RL was determined (N=3 for each stage).

Statistical analysis: We applied a Chi-square test to compare proportions of ventricular and basal progenitors in the mouse, human VZ/SVZ, and $RL^{VZ/SVZ}$ at different stages of development. Differences observed between groups were determined by Prism7. The Chi-square test shows that the difference in proportions observed between ventricular and basal progenitors at different stages and in the different regions are not due to the data variability. To determine if there was a significant difference in the RL KI67 and SOX2+ populations between 14 and 17pcw (N=3 per age), t-test was applied. Data is represented as mean +/- SEM. Statistical analysis was done using excel. P values are mentioned in the figure legends.

Supplementary Figures: Figure S1

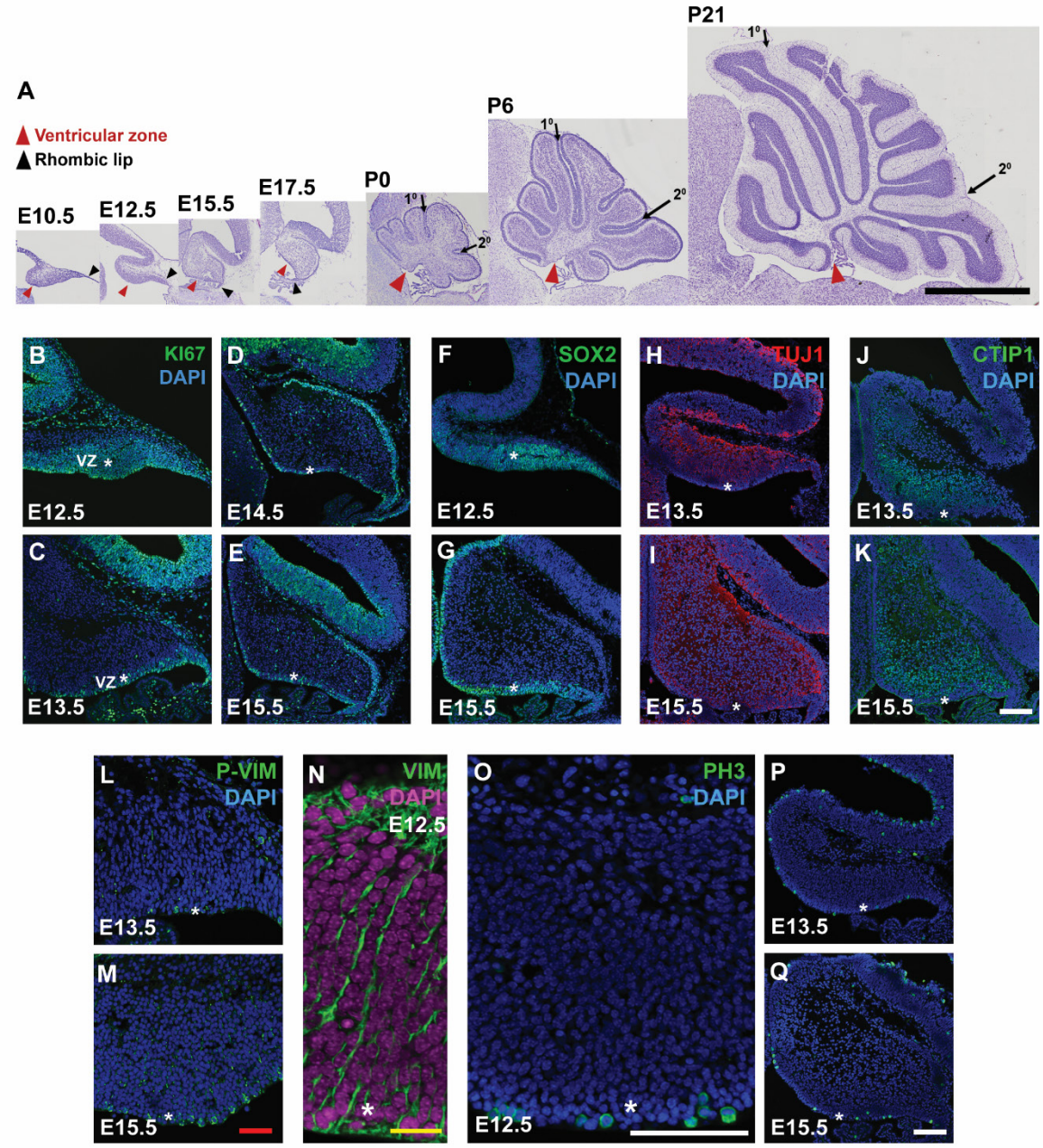

Fig. S1: An outline of mouse cerebellar development. Cresyl violet-stained midsagittal sections through the mouse embryonic (E10.5-E17.5) and postnatal (P0-P21) cerebellum indicates the transient presence of the ventricular zone (red arrowhead) and rhombic lip (black arrow head). Primary and secondary fissures are noted (arrows). KI67 (B-E) and SOX2 (F-G) staining indicate the cerebellar VZ shrinks in thickness after E12.5, with a 2-4 cell layer thick structure lining the ventricle. Neuronal differentiation takes place directly above the VZ as indicated by TUJ1 (H-I) and CTIP1 (J-K) expression. Expression of phospho-Vimentin (L,M) – which marks mitotic radial glia, and phospho-histone- H3 (O-Q, PH3) which marks all cells in mitosis reveal that mitosis is only confined to the cerebellar VZ thus indicating the lack of a subventricular zone in the mouse cerebellum. Radial glial fibers span the length of the cerebellar anlage as evinced by vimentin staining (N). VZ is indicated by a white asterisk in B-Q. Scale bar = 100 µm (A-K, O-Q, black/white), 50 µm (L-M, red) and 20 µm (N, yellow).

Figure S2

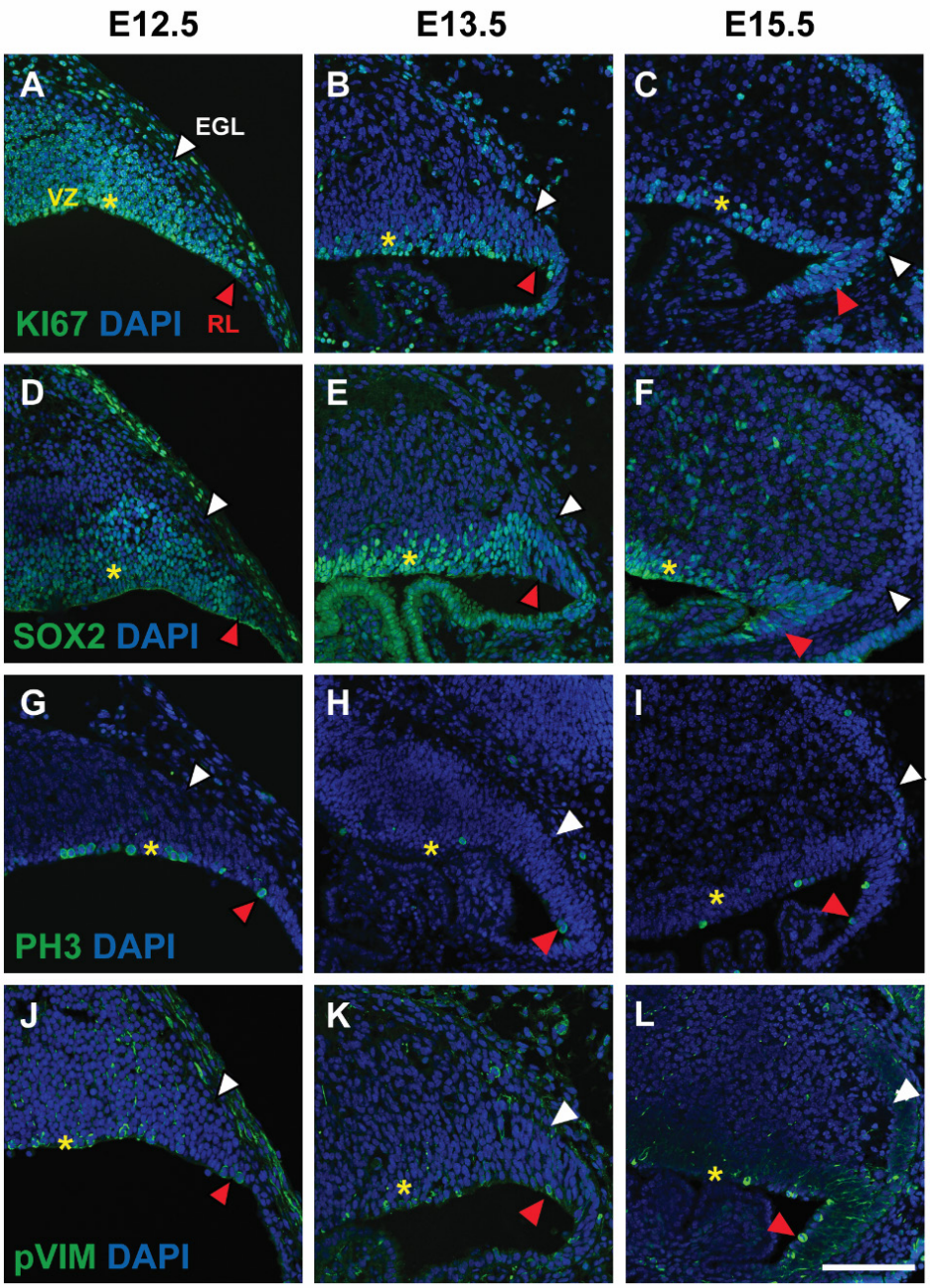

Fig. S2: Rhombic lip development in the mouse. Expression of KI67 (A-C) and SOX2 (D-F) throughout the mouse cerebellar RL (red arrowhead) shows that the RL in mouse consists of multiple layers of proliferative cells and lacks structural compartmentalization. Expression of phospho-histone H3 (G-I; red arrowhead) and phospho-Vimentin (J-L) shows mitosis is only confined to the layer of RL cells lining the ventricle (red arrowhead). Mitosis is also exhibited once cells exit the RL and enter the EGL (G-L white arrowhead). VZ is indicated by a yellow asterisk. Scale bar = 100 μm

Figure S3

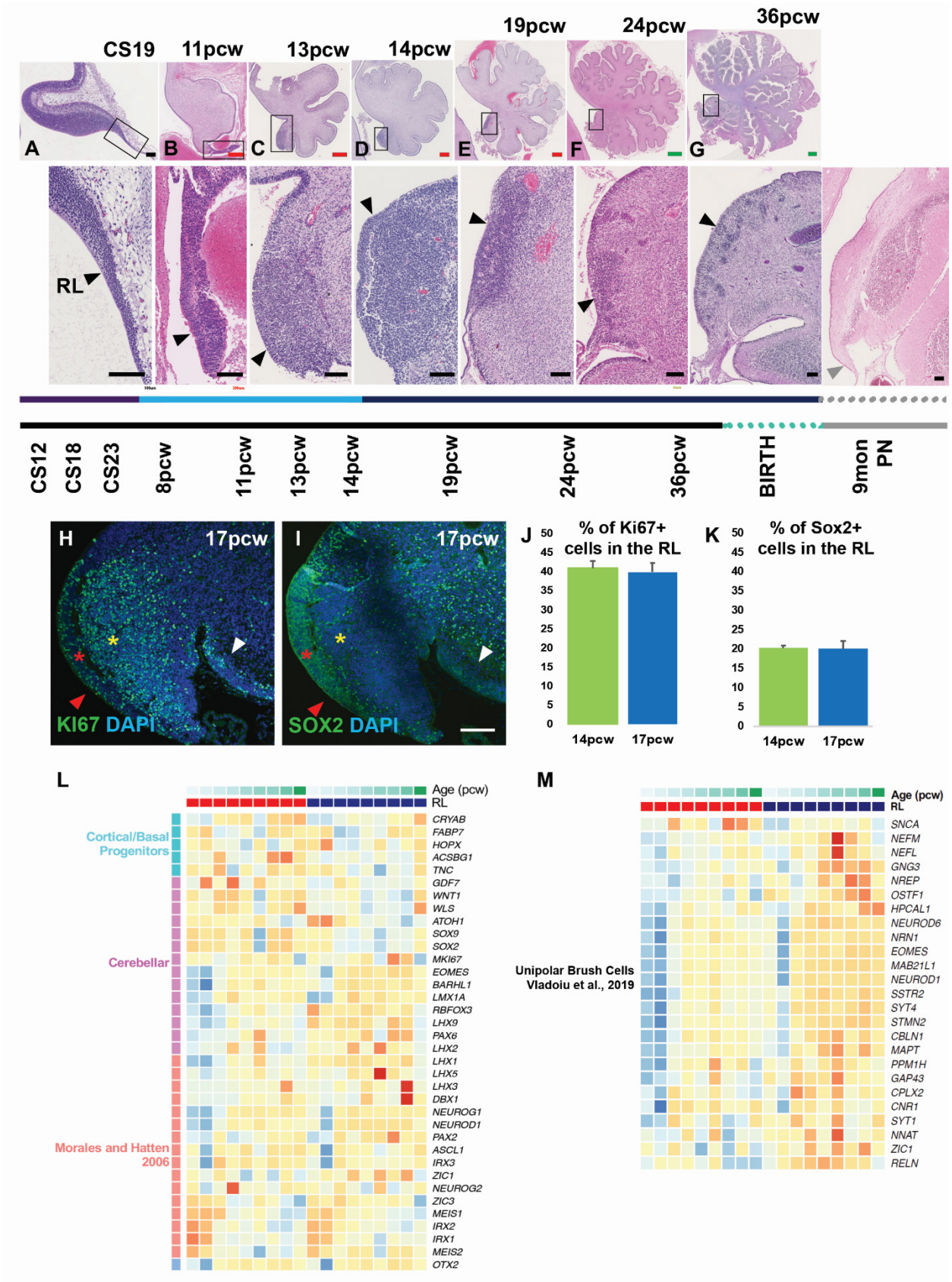
CS19
11pcw
13pcw
14pcw
19pcw
24pcw
36pcw
A
B
C
D
E
F
G
RL
CS12
CS18
CS23
8pcw
11pcw
13pcw
14pcw
19pcw
24pcw
36pcw
BIRTH
9mon PN
H
17pcw
KI67 DAPI
I
17pcw
SOX2 DAPI
J
% of Ki67+ cells in the RL
14pcw
17pcw
K
% of Sox2+ cells in the RL
14pcw
17pcw
L
Age (pcw)
RL
Cortical/Basal Progenitors
Cerebellar
Morales and Hatten 2006
CRYAB
FABP7
HOPX
ACSBG1
TNC
GDF7
WNT1
WLS
ATOH1
SOX9
SOX2
MKI67
EOMES
BARHL1
LMX1A
RBFOX3
LHX9
PAX6
LHX2
LHX1
LHX5
LHX3
DBX1
NEUROG1
NEUROD1
PAX2
ASCL1
IRX3
ZIC1
NEUROG2
ZIC3
MEIS1
IRX2
IRX1
MEIS2
OTX2
M
Age (pcw)
RL
Unipolar Brush Cells Vladoiu et al., 2019
SNCA
NEFM
NEFL
GNG3
NREP
OSTF1
HPCAL1
NEUROD6
NRN1
EOMES
MAB21L1
NEUROD1
SSTR2
SYT4
STMN2
CBLN1
MAPT
PPM1H
GAP43
CPLX2
CNR1
SYT1
NNAT
ZIC1
RELN

Fig. S3: Spatiotemporal expansion of the human rhombic lip. The human cerebellar RL undergoes morphological transformations during development and provides granule cell progenitors to the external granule layer. The human RL (black arrowhead) structurally resembles the mouse RL at CS19 (A). Between 8 and 12 pcw, it is elongated into a 'tail-like' structure (B, box). (C-G, box) After 13 pcw the RL internalizes to form a pool of cells confined to the posterior-most lobule until birth. KI67 (H) and SOX2 (I) expression in the 17pcw RL (red arrowhead), reveal no significant difference in proliferation (J; t-test, p value = 0.9862) or SOX2+ cell numbers (K; t-test, p value = 0.9638) between 14 and 17pcw. Data is represented as Mean +/- SEM. Granule cell progenitors can be seen streaming into the external granule layer (H-I, white arrowhead). (L) Heatmap of gene expression of cortical basal progenitors, mouse cerebellar genes, including from *Morales and Hatten 2006 (22)* and (M) Unipolar brush cells-genes from *Vladoiu et al., 2019 (23)*. Samples are grouped by RL compartment (RL^{VZ} labeled red and RL^{SVZ} labeled blue), then ascending age (9 to 22 pcw). Expression Z-score from high (red) to low (blue). Scale bar = 100 µm (A, black; H, I, white), 500 µm (B-E, red), and 1 mm (F, G, green).

Figure S4

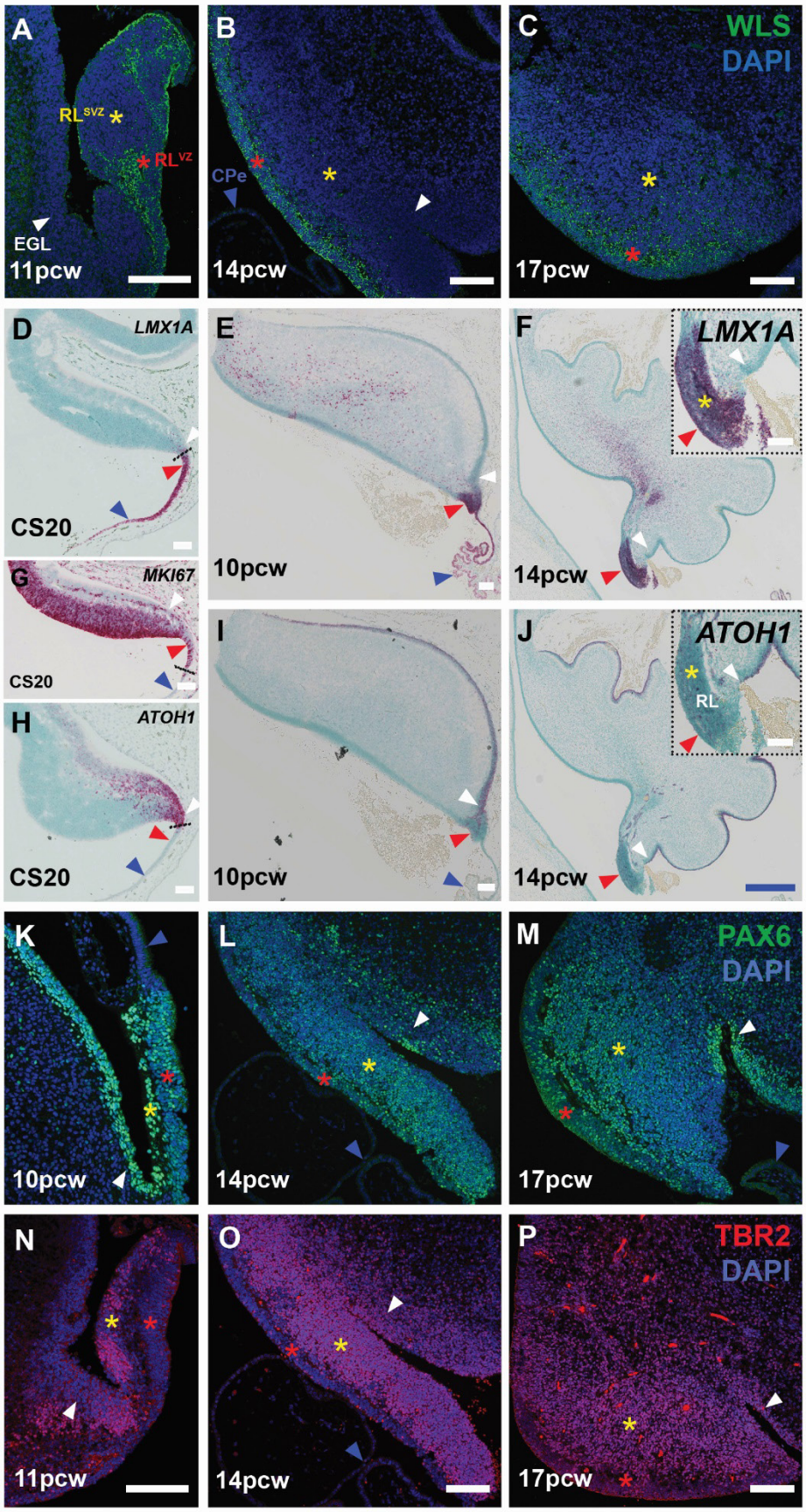
A
RL SVZ
RL VZ
EGL
11pcw
B
CPe
14pcw
C
WLS
DAPI
17pcw
D
LMX1A
CS20
E
10pcw
F
LMX1A
14pcw
G
MKI67
CS20
H
ATOH1
CS20
I
10pcw
J
ATOH1
RL
14pcw
K
10pcw
L
14pcw
M
PAX6
DAPI
17pcw
N
11pcw
O
14pcw
P
TBR2
DAPI
17pcw

Fig. S4: Expression of selected genes in the human cerebellar rhombic lip. Wntless (A-C) expression in the human RL. *LMX1A* (D-F) and *ATOH1* (H-J) expression as detected by *in situ* hybridization can be used to define the boundary between the RL (red arrowhead) and EGL (white arrowhead), with LMX1A marking all RL and Unipolar brush cells that migrate into the cerebellar anlage core, and ATOH1 specifically marking cells exiting the RL and specifically the granule cell precursors of the EGL. *MKI67* expression defines the boundary of the rhombic lip and choroid plexus epithelium (G, black line, blue arrowhead). PAX6 (K-M) and TBR2 (N-P) which are highly expressed in the mouse RL are also expressed in the human RL. The RL shows high expression of PAX6 in both the RL^{VZ} (red asterisk) and RL^{SVZ} (yellow asterisk). PAX6 expression persists in all RL derivatives including the GCPs of the EGL (K-M). WLS and TBR2 on the other hand are differentially expressed in the RL^{VZ} (A-C, red asterisk) and RL^{SVZ} (N-P, yellow asterisk) respectively. Sections processed for immunohistochemistry and *in situ* hybridization were counterstained with DAPI and fast green respectively. Scale bar = 100 μm (white), 500 μm (F, J, blue).

Figure S5

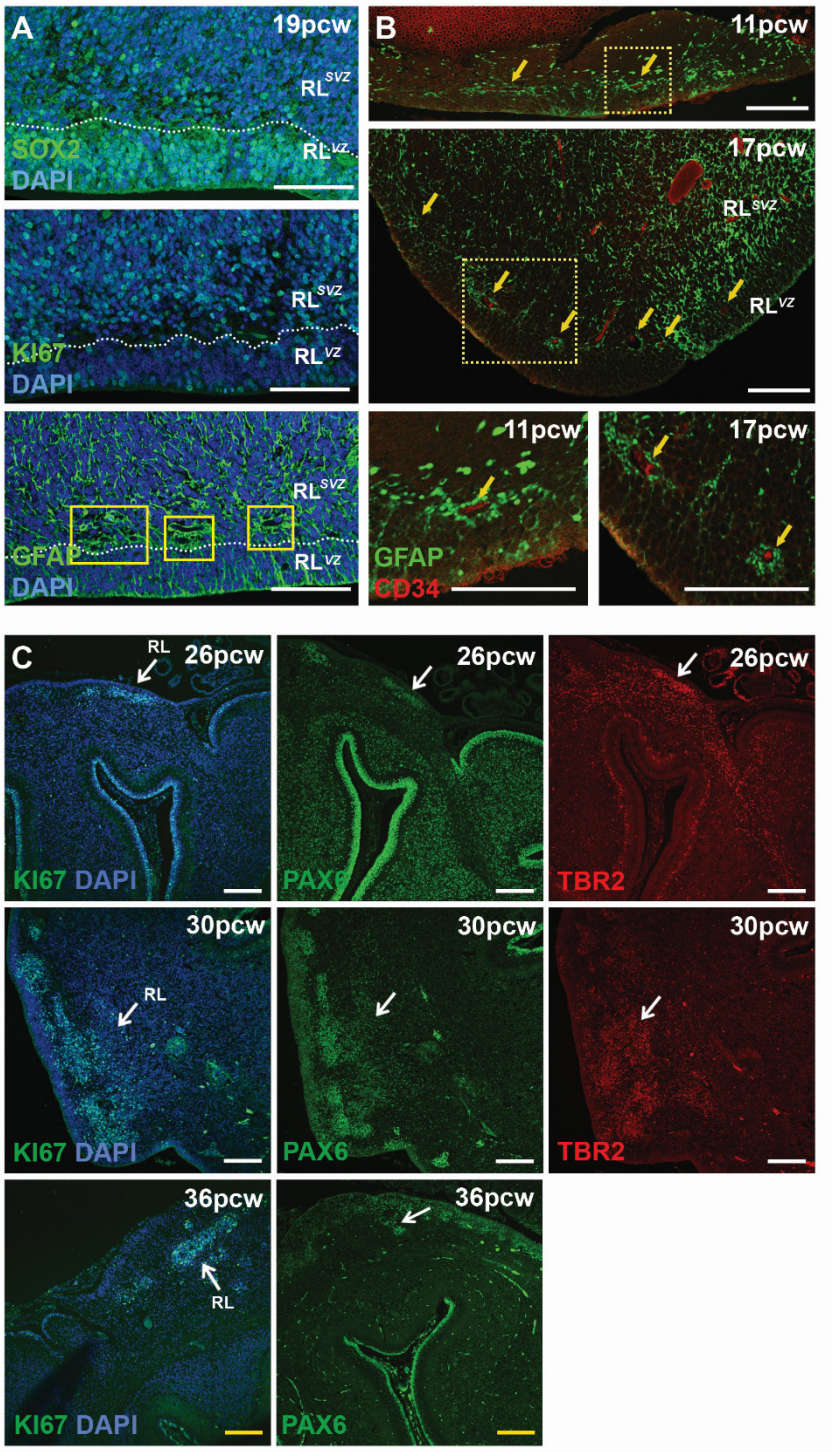

Fig. S5: The human rhombic lip is a highly vascularized region and persists until birth. The human cerebellar RL is structurally compartmentalized into a ventricular (RL^{VZ}) and subventricular zones (RL^{SVZ}) (A). The two compartments are separated by a lining of blood vessels and glia as indicated by GFAP (A, B) and CD34 expression (B, arrows). Although the structure of the rhombic lip changes over time, it persists until birth as indicated by KI67, PAX6 and TBR2 staining (C, arrows). Scale bar = 100 µm (white) and 200 µm (yellow).

Figure S6

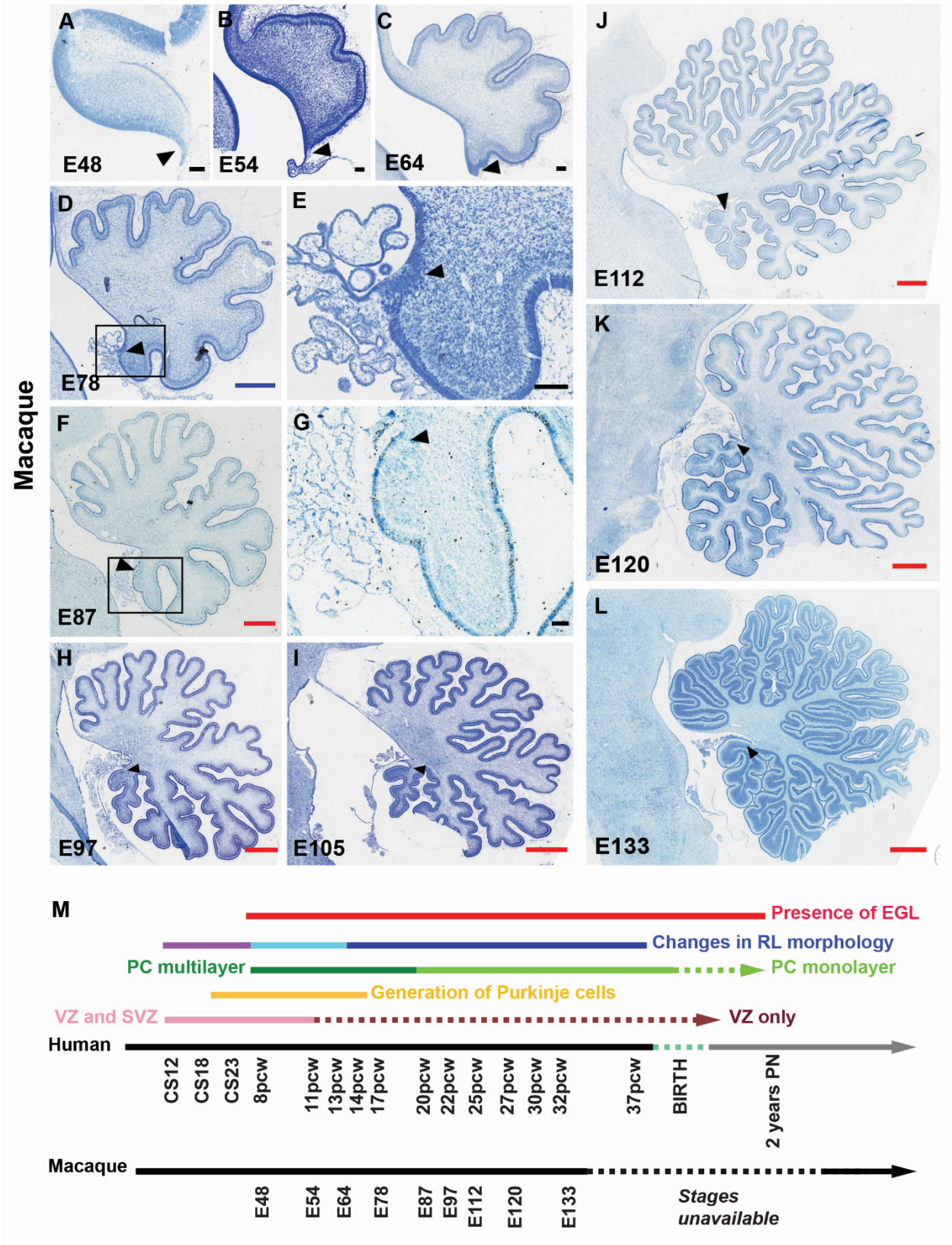
Macaque
A
E48
B
E54
C
E64
D
E78
E
F
E87
G
H
E97
I
E105
J
E112
K
E120
L
E133
M
Presence of EGL
Changes in RL morphology
PC multilayer
PC monolayer
Generation of Purkinje cells
VZ and SVZ
VZ only
Human
CS12
CS18
CS23
8pcw
11pcw
13pcw
14pcw
17pcw
20pcw
22pcw
25pcw
27pcw
30pcw
32pcw
37pcw
BIRTH
2 years PN
Macaque
E48
E54
E64
E78
E87
E97
E112
E120
E133
Stages unavailable

Fig. S6: Internalized rhombic lip is a feature specific to human cerebellar development. Cresyl violet-stained sagittal sections of the developing macaque cerebellum at (A) Embryonic day [E] 48, (B) E54, (C) E64, (D, E) E78, (F, G) E87, (H) E97, (I) E105, (J) E112, (K) E120 and (L) E133 suggests that the internalized rhombic lip is not a feature of macaques, but rather a human-specific trait. (M) A comparative timeline of human and macaque cerebellar development based on folial complexity and histogenesis. Data post E133 are unavailable. Scale bar = 100 μm (black), 0.5 mm (blue) and 1 mm (red).

Figure S7

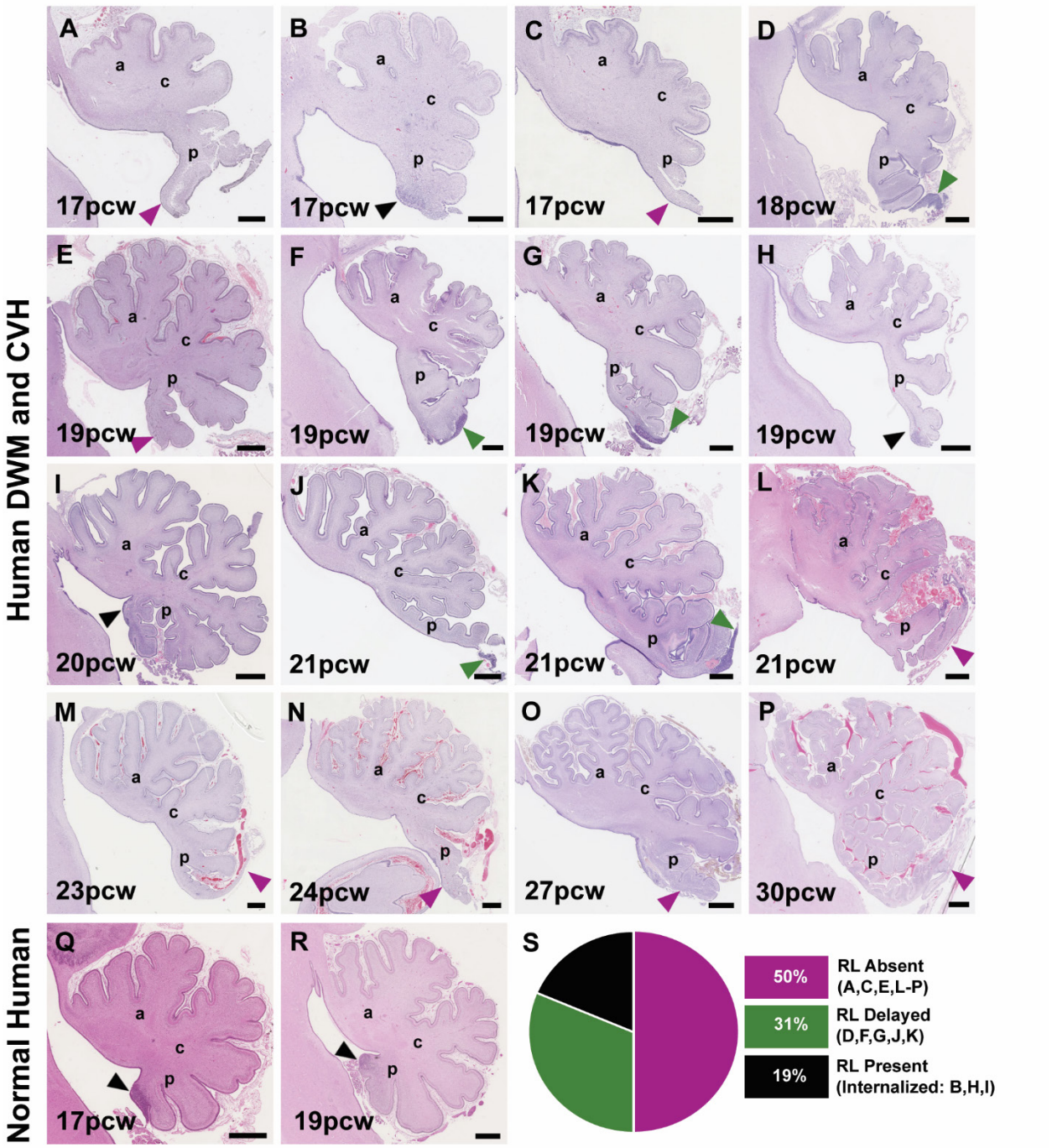

Fig. S7: Disruption in rhombic lip development is associated with cerebellar hypoplasia. (A-P) Analysis of H&E-stained sagittal sections of the human cerebellum from 16 cases diagnosed with Dandy Walker malformation [DWM] (A-D, F-H, J-P) and cerebellar vermis hypoplasia [CVH] (E, I) indicates the RL is absent in 50% of cases while in the remaining cases it is severely diminished (S). (Q, R) H&E-stained sections of the normal cerebellum. (S) Pie chart representing the absence of rhombic lip in 50% of tested samples. The anterior (a), central (c) and posterior lobes (p) are indicated. Absent, delayed and internalized RL are indicated by magenta, green and black arrowheads. Scale bar = 1 mm. *Note: Images H, K, M and T have been included in Figure 6. Cases A and E have been used previously in Haldipur et al., 2017 (31).*

Table S1: List of samples used in the study

Species	Age	Number of samples	Type
Human	CS12 (30days post-conception)	1	Normal
Human	CS14 (33d)	2	Normal
Human	CS16 (39d)	3	Normal
Human	CS17 (41d)	1	Normal
Human	CS18 (44d)	3	Normal
Human	CS19 (46d)	3	Normal
Human	CS20 (49d)	3	Normal
Human	CS21 (51d)	2	Normal
Human	CS22 (53d)	2	Normal
Human	CS23 (56d)	3	Normal
Human	8 pcw	1	Normal
Human	9 pcw	2	Normal
Human	10 pcw	3	Normal
Human	11 pcw	4	Normal
Human	12 pcw	3	Normal
Human	13 pcw	4	Normal
Human	14 pcw	6	Normal
Human	15 pcw	2	Normal
Human	16 pcw	2	Normal
Human	17 pcw	6	Normal
Human	18 pcw	5	Normal
Human	19 pcw	4	Normal
Human	20-24 pcw	8	Normal
Human	25-32 pcw	6	Normal
Human	33-40 pcw	5	Normal
Human	17 pcw	3	Dandy Walker malformation
Human	18 pcw	1	Dandy Walker malformation
Human	19 pcw	3	Dandy Walker malformation
Human	19 pcw	1	Cerebellar vermis hypoplasia
Human	20 pcw	1	Cerebellar vermis hypoplasia
Human	21 pcw	3	Dandy Walker malformation
Human	23 pcw	1	Dandy Walker malformation
Human	24 pcw	1	Dandy Walker malformation
Human	27 pcw	1	Dandy Walker malformation
Human	30 pcw	1	Dandy Walker malformation
Rhesus macaque	Embryonic day 48	1	Normal
Rhesus macaque	Embryonic day 54	1	Normal
Rhesus macaque	Embryonic day 64	1	Normal
Rhesus macaque	Embryonic day 78	1	Normal
Rhesus macaque	Embryonic day 87	1	Normal
Rhesus macaque	Embryonic day 97	1	Normal
Rhesus macaque	Embryonic day 105	1	Normal
Rhesus macaque	Embryonic day 112	1	Normal
Rhesus macaque	Embryonic day 120	1	Normal
Rhesus macaque	Embryonic day 133	1	Normal

Data S1-S4. (separate file)

Data S1: List of samples used for RNA seq analysis
Data S2: Rhombic lip transcriptome differential gene expression analysis
Data S3: Biological process and pathway enrichment among RL^{VZ} genes
Data S4: Biological process enrichment among RL^{SVZ} genes

References and Notes

1. W. Lange, Cell number and cell density in the cerebellar cortex of man and some other mammals. *Cell Tissue Res.* **157**, 115–124 (1975). doi:10.1007/BF00223234 Medline

2. D. C. Van Essen, Surface-based atlases of cerebellar cortex in the human, macaque, and mouse. *Ann. N. Y. Acad. Sci.* **978**, 468–479 (2002). doi:10.1111/j.1749-6632.2002.tb07588.x Medline

3. O. Larsell, J. Jansen, *The Comparative Anatomy and Histology of the Cerebellum. The Human Cerebellum, Cerebellar Connections, and Cerebellar Cortex* (Univ. of Minnesota Press, 1972).

4. P. Haldipur, U. Bharti, C. Alberti, C. Sarkar, G. Gulati, S. Iyengar, P. Gressens, S. Mani, Preterm delivery disrupts the developmental program of the cerebellum. *PLOS ONE* **6**, e23449 (2011). doi:10.1371/journal.pone.0023449 Medline

5. P. Rakic, R. L. Sidman, Histogenesis of cortical layers in human cerebellum, particularly the lamina dissecans. *J. Comp. Neurol.* **139**, 473–500 (1970). doi:10.1002/cne.901390407 Medline

6. Z. Molnár, A. Pollen, How unique is the human neocortex? *Development* **141**, 11–16 (2014). doi:10.1242/dev.101279 Medline

7. T. J. Nowakowski, A. A. Pollen, C. Sandoval-Espinosa, A. R. Kriegstein, Transformation of the radial glia scaffold demarcates two stages of human cerebral cortex development. *Neuron* **91**, 1219–1227 (2016). doi:10.1016/j.neuron.2016.09.005 Medline

8. S. Herculano-Houzel, Coordinated scaling of cortical and cerebellar numbers of neurons. *Front. Neuroanat.* **4**, 12 (2010). Medline

9. O. Larsell, W. A. Stotler, Some morphological features of the human cerebellum. *Anat. Rec.* **97**, 352 (1947). Medline

10. H. Ábrahám, T. Tornóczky, G. Kosztolányi, L. Seress, Cell formation in the cortical layers of the developing human cerebellum. *Int. J. Dev. Neurosci.* **19**, 53–62 (2001). doi:10.1016/S0736-5748(00)00065-4 Medline

11. P. Haldipur, U. Bharti, S. Govindan, C. Sarkar, S. Iyengar, P. Gressens, S. Mani, Expression of Sonic hedgehog during cell proliferation in the human cerebellum. *Stem Cells Dev.* **21**, 1059–1068 (2012). doi:10.1089/scd.2011.0206 Medline

12. N. Zecevic, P. Rakic, Differentiation of Purkinje cells and their relationship to other components of developing cerebellar cortex in man. *J. Comp. Neurol.* **167**, 27–47 (1976). doi:10.1002/cne.901670103 Medline

13. P. A. Habas, K. Kim, J. M. Corbett-Detig, F. Rousseau, O. A. Glenn, A. J. Barkovich, C. Studholme, A spatiotemporal atlas of MR intensity, tissue probability and shape of the fetal brain with application to segmentation. *Neuroimage* **53**, 460–470 (2010). doi:10.1016/j.neuroimage.2010.06.054 Medline

14. K. Leto, M. Arancillo, E. B. E. Becker, A. Buffo, C. Chiang, B. Ding, W. B. Dobyns, I. Dusart, P. Haldipur, M. E. Hatten, M. Hoshino, A. L. Joyner, M. Kano, D. L. Kilpatrick, N. Koibuchi, S. Marino, S. Martinez, K. J. Millen, T. O. Millner, T. Miyata, E.

Parmigiani, K. Schilling, G. Sekerková, R. V. Sillitoe, C. Sotelo, N. Uesaka, A. Wefers, R. J. T. Wingate, R. Hawkes, Consensus paper: Cerebellar development. *Cerebellum* **15**, 789–828 (2016). doi:10.1007/s12311-015-0724-2 Medline

15. J. D. Corrales, G. L. Rocco, S. Blaess, Q. Guo, A. L. Joyner, Spatial pattern of sonic hedgehog signaling through Gli genes during cerebellum development. *Development* **131**, 5581–5590 (2004). doi:10.1242/dev.01438 Medline

16. N. Dahmane, A. Ruiz i Altaba, Sonic hedgehog regulates the growth and patterning of the cerebellum. *Development* **126**, 3089–3100 (1999). Medline

17. C. Limperopoulos, J. S. Soul, K. Gauvreau, P. S. Huppi, S. K. Warfield, H. Bassan, R. L. Robertson, J. J. Volpe, A. J. du Plessis, Late gestation cerebellar growth is rapid and impeded by premature birth. *Pediatrics* **115**, 688–695 (2005). doi:10.1542/peds.2004-1169 Medline

18. J. J. Volpe, Cerebellum of the premature infant: Rapidly developing, vulnerable, clinically important. *J. Child Neurol.* **24**, 1085–1104 (2009). doi:10.1177/0883073809338067 Medline

19. A. A. Pollen, T. J. Nowakowski, J. Chen, H. Retallack, C. Sandoval-Espinosa, C. R. Nicholas, J. Shuga, S. J. Liu, M. C. Oldham, A. Diaz, D. A. Lim, A. A. Leyrat, J. A. West, A. R. Kriegstein, Molecular identity of human outer radial glia during cortical development. *Cell* **163**, 55–67 (2015). doi:10.1016/j.cell.2015.09.004 Medline

20. V. V. Chizhikov, A. G. Lindgren, Y. Mishima, R. W. Roberts, K. A. Aldinger, G. R. Miesegaes, D. S. Currle, E. S. Monuki, K. J. Millen, Lmx1a regulates fates and location of cells originating from the cerebellar rhombic lip and telencephalic cortical hem. *Proc. Natl. Acad. Sci. U.S.A.* **107**, 10725–10730 (2010). doi:10.1073/pnas.0910786107 Medline

21. J. Yeung, T. J. Ha, D. J. Swanson, K. Choi, Y. Tong, D. Goldowitz, *Wls* provides a new compartmental view of the rhombic lip in mouse cerebellar development. *J. Neurosci.* **34**, 12527–12537 (2014). doi:10.1523/JNEUROSCI.1330-14.2014 Medline

22. D. Morales, M. E. Hatten, Molecular markers of neuronal progenitors in the embryonic cerebellar anlage. *J. Neurosci.* **26**, 12226–12236 (2006). doi:10.1523/JNEUROSCI.3493-06.2006 Medline

23. M. C. Vladoiu, I. El-Hamamy, L. K. Donovan, H. Farooq, B. L. Holgado, Y. Sundaravadanam, V. Ramaswamy, L. D. Hendrikse, S. Kumar, S. C. Mack, J. J. Y. Lee, V. Fong, K. Juraschka, D. Przelicki, A. Michealraj, P. Skowron, B. Luu, H. Suzuki, A. S. Morrissy, F. M. G. Cavalli, L. Garzia, C. Daniels, X. Wu, M. A. Qazi, S. K. Singh, J. A. Chan, M. A. Marra, D. Malkin, P. Dirks, L. Heisler, T. Pugh, K. Ng, F. Notta, E. M. Thompson, C. L. Kleinman, A. L. Joyner, N. Jabado, L. Stein, M. D. Taylor, Childhood cerebellar tumours mirror conserved fetal transcriptional programs. *Nature* **572**, 67–73 (2019). doi:10.1038/s41586-019-1158-7 Medline

24. J. W. Wizeman, Q. Guo, E. M. Wilion, J. Y. Li, Specification of diverse cell types during early neurogenesis of the mouse cerebellum. *eLife* **8**, e42388 (2019). doi:10.7554/eLife.42388 Medline

25. M. Florio, W. B. Huttner, Neural progenitors, neurogenesis and the evolution of the neocortex. *Development* **141**, 2182–2194 (2014). doi:10.1242/dev.090571 Medline

26. J. H. Lui, D. V. Hansen, A. R. Kriegstein, Development and evolution of the human neocortex. *Cell* **146**, 18–36 (2011). doi:10.1016/j.cell.2011.06.030 Medline

27. F. A. Azevedo, L. R. B. Carvalho, L. T. Grinberg, J. M. Farfel, R. E. L. Ferretti, R. E. P. Leite, W. Jacob Filho, R. Lent, S. Herculano-Houzel, Equal numbers of neuronal and nonneuronal cells make the human brain an isometrically scaled-up primate brain. *J. Comp. Neurol.* **513**, 532–541 (2009). doi:10.1002/cne.21974 Medline

28. S. Herculano-Houzel, The human brain in numbers: A linearly scaled-up primate brain. *Front. Hum. Neurosci.* **3**, 31 (2009). doi:10.3389/neuro.09.031.2009 Medline

29. A. J. Barkovich, K. J. Millen, W. B. Dobyns, A developmental and genetic classification for midbrain-hindbrain malformations. *Brain* **132**, 3199–3230 (2009). doi:10.1093/brain/awp247 Medline

30. K. A. Aldinger, O. J. Lehmann, L. Hudgins, V. V. Chizhikov, A. G. Bassuk, L. C. Ades, I. D. Krantz, W. B. Dobyns, K. J. Millen, *FOXC1* is required for normal cerebellar development and is a major contributor to chromosome 6p25.3 Dandy-Walker malformation. *Nat. Genet.* **41**, 1037–1042 (2009). doi:10.1038/ng.422 Medline

31. P. Haldipur, D. Dang, K. A. Aldinger, O. K. Janson, F. Guimiot, H. Adle-Biasette, W. B. Dobyns, J. R. Siebert, R. Russo, K. J. Millen, Phenotypic outcomes in Mouse and Human *Foxc1* dependent Dandy-Walker cerebellar malformation suggest shared mechanisms. *eLife* **6**, e20898 (2017). doi:10.7554/eLife.20898 Medline

32. P. Haldipur, G. S. Gillies, O. K. Janson, V. V. Chizhikov, D. S. Mithal, R. J. Miller, K. J. Millen, Foxc1 dependent mesenchymal signalling drives embryonic cerebellar growth. *eLife* **3**, e03962 (2014). doi:10.7554/eLife.03962 Medline

33. J. D. Schmahmann, X. Guell, C. J. Stoodley, M. A. Halko, The theory and neuroscience of cerebellar cognition. *Annu. Rev. Neurosci.* **42**, 337–364 (2019). doi:10.1146/annurev-neuro-070918-050258 Medline

34. S. Bernardo, V. Vinci, M. Saldari, F. Servadei, E. Silvestri, A. Giancotti, C. Aliberti, M. G. Porpora, F. Triulzi, G. Rizzo, C. Catalano, L. Manganaro, Dandy-Walker malformation: Is the 'tail sign' the key sign? *Prenat. Diagn.* **35**, 1358–1364 (2015). doi:10.1002/pd.4705 Medline

35. A. Poretti, E. Boltshauser, T. A. G. M. Huisman, Pre- and postnatal neuroimaging of congenital cerebellar abnormalities. *Cerebellum* **15**, 5–9 (2016). doi:10.1007/s12311-015-0699-z Medline

36. K. A. Aldinger, A. E. Timms, Z. Thomson, G. M. Mirzaa, J. T. Bennett, A. B. Rosenberg, C. M. Roco, M. Hirano, F. Abidi, P. Haldipur, C. V. Cheng, S. Collins, K. Park, J. Zeiger, L. M. Overmann, F. S. Alkuraya, L. G. Biesecker, S. R. Braddock, S. Cathey, M. T. Cho, B. H. Y. Chung, D. B. Everman, Y. A. Zarate, J. R. Jones, C. E. Schwartz, A. Goldstein, R. J. Hopkin, I. D. Krantz, R. L. Ladda, K. A. Leppig, B. C. McGillivray, S. Sell, K. Wusik, J. G. Gleeson, D. A. Nickerson, M. J. Bamshad, D. Gerrelli, S. N. Lisgo, G. Seelig, G. E. Ishak, A. J. Barkovich, C. J. Curry, I. A. Glass, K. J. Millen, D. Doherty, W. B. Dobyns, Redefining the etiologic landscape of cerebellar malformations. *Am. J. Hum. Genet.* **105**, 606–615 (2019). doi:10.1016/j.ajhg.2019.07.019 Medline

37. A. Pichiecchio, A. Decio, C. Di Perri, C. Parazzini, A. Rossi, S. Signorini, “Acquired” Dandy-Walker malformation and cerebellar hemorrhage: Usefulness of serial MRI. *Eur. J. Paediatr. Neurol.* **20**, 188–191 (2016). doi:10.1016/j.ejpn.2015.09.009 Medline

38. R. Azzarelli, B. D. Simons, A. Philpott, The developmental origin of brain tumours: A cellular and molecular framework. *Development* **145**, dev162693 (2018). doi:10.1242/dev.162693 Medline

39. K. Saito, A. Kawaguchi, S. Kashiwagi, S. Yasugi, M. Ogawa, T. Miyata, Morphological asymmetry in dividing retinal progenitor cells. *Dev. Growth Differ.* **45**, 219–229 (2003). doi:10.1046/j.1524-4725.2003.690.x Medline

40. F. Zhang, S. I. Thornhill, S. J. Howe, M. Ulaganathan, A. Schambach, J. Sinclair, C. Kinnon, H. B. Gaspar, M. Antoniou, A. J. Thrasher, Lentiviral vectors containing an enhancer-less ubiquitously acting chromatin opening element (UCOE) provide highly reproducible and stable transgene expression in hematopoietic cells. *Blood* **110**, 1448–1457 (2007). doi:10.1182/blood-2006-12-060814 Medline

41. A. Dobin, C. A. Davis, F. Schlesinger, J. Drenkow, C. Zaleski, S. Jha, P. Batut, M. Chaisson, T. R. Gingeras, STAR: Ultrafast universal RNA-seq aligner. *Bioinformatics* **29**, 15–21 (2013). doi:10.1093/bioinformatics/bts635 Medline

42. S. Anders, P. T. Pyl, W. Huber, HTSeq—A Python framework to work with high-throughput sequencing data. *Bioinformatics* **31**, 166–169 (2015). doi:10.1093/bioinformatics/btu638 Medline

43. M. I. Love, W. Huber, S. Anders, Moderated estimation of fold change and dispersion for RNA-seq data with DESeq2. *Genome Biol.* **15**, 550 (2014). doi:10.1186/s13059-014-0550-8 Medline

44. D. Szklarczyk, A. L. Gable, D. Lyon, A. Junge, S. Wyder, J. Huerta-Cepas, M. Simonovic, N. T. Doncheva, J. H. Morris, P. Bork, L. J. Jensen, C. V. Mering, STRING v11: Protein-protein association networks with increased coverage, supporting functional discovery in genome-wide experimental datasets. *Nucleic Acids Res.* **47**, D607–D613 (2019). doi:10.1093/nar/gky1131 Medline

45. F. Supek, M. Bošnjak, N. Škunca, T. Šmuc, REVIGO summarizes and visualizes long lists of gene ontology terms. *PLOS ONE* **6**, e21800 (2011). doi:10.1371/journal.pone.0021800 Medline